Eur. Phys. J. D **8**, 403–416 (2000)

THE EUROPEAN PHYSICAL JOURNAL D

EDP Sciences

Bistable behaviour in squeezed vacua: I. Stationary analysis

S.S. Hassan[1], H.A. Batarfi[2], R. Saunders[3], and R.K. Bullough[4]

[1] Ain Shams University, Faculty of Science, Mathematics Department, Cairo, Egypt
[2] King Abdul-Aziz University, Faculty of Science, Mathematics Department (Women's Section), P.O. Box 41101, Jeddah 21521, Saudi Arabia
[3] Department of Mathematics and Physics, Manchester Metropolitan University, Manchester M1 5GD, England
[4] UMIST, Mathematics Department, P.O. Box 88, Manchester M60 1QD, England

Received 12 March 1999 and Received in final form 20 August 1999

Abstract. A time-independent theoretical and numerical analysis of an optical bistable model of two-level atoms in a ring cavity, driven by a coherent field and in contact with a squeezed vacuum field is presented in the two cases of absorptive and dispersive optical bistability (OB). In the former case, a suitable choice of the phase of the squeezed vacuum field reduces the threshold for OB to occur compared with the normal vacuum case. In the latter case, regions of OB are identified as one or two disconnected simple closed curves depending on the cooperation parameter $C \gtrless C_{\rm crit}^{\rm max}$: $C_{\rm crit}^{\rm max}$ is the maximum possible value of the critical value of C at fixed values of the squeezed vacuum field parameters. Phase switching effects between different (output) states of the system is investigated in detail. In the absorptive case, one- or two-way optical switching is possible depending on $C \gtrless C_{\rm crit}^{\rm max}$. We also present results which demonstrate more complicated switching behaviour in the dispersive case.

PACS. 42.65.Pc Optical bistability, multistability, and switching – 42.65.Sf Dynamics of nonlinear optical systems, optical instabilities and optical chaos and complexity, and optical spatio-temporal dynamics

1 Introduction

Dynamical study of non-linear optical systems is an active research area for its fundamental aspect as well for its potential technological applications in the real world [1]. A particular example is the phenomena of optical bistability (OB) which has potential applications in optical communications and the quantum processing of information (*e.g.* [1–4]). OB is caused by the non-unique response of an optical feedback system for which there are two possible stable outputs from the system. The phenomenon has been examined, both theoretically and experimentally, in various optical cavity configurations ([1–6]; and the extensive references therein). On the other hand "squeezing" of the electromagnetic field vacuum fluctuations, where the quantum fluctuations in one-quadrature phase of the field are less than the usual vacuum fluctuations, has been realised for some years (for latest experimental developments see [7,8] and see [9,10] for intensive literature on the properties of squeezed light and its use to prope non-linear optical systems). Of relevant interest is the interaction of 2-level atomic systems with a broad-band squeezed vacuum field which induces two different decay rates for the quadrature components of the atomic polarization, and also broadens the decay rate of the atomic population [11].

Theoretical investigation of (a single mode) OB system in a ring cavity configuration (Fig. 1) where the atomic system is in interaction with a squeezed vacuum input field

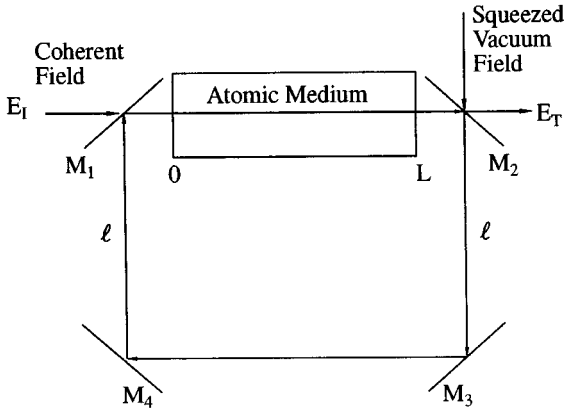

Fig. 1. The ring cavity configuration.

have been given (to our knowledge) in [12–14]. In [12] the degradation of the bistable behaviour due to the squeezed vacuum parameters was examined in the absorptive case (no cavity detuning), while the authors of [13] have discussed the use of the squeezed light input field to produce a "switching effect" in an optical bistable system by varying the phase of the squeezed light. The authors of [14] have investigated an absorptive bistable system (both cavity and atomic detunings are zero) in a ring cavity (Fig. 1) where the squeezed vacuum beam is introduced at the mirror M_2: this has the (experimental) advantage to avoid phase mis-match and diffraction problems discussed

in [12,13], and also to neglect the coupling between the cavity field and the squeezed vacuum field.

In this two-part article we present the full theoretical and numerical analysis for an OB system of 2-level atoms in a ring cavity where the atoms are coupled to the squeezed vacuum field, injected at mirror M_2 of Figure 1, while the incident coherent field $E_{\rm I}$ is injected at mirror M_1 (just as in [14]) and it is detuned to both cavity and atoms. In the first part of this article we present a steady state analysis of the input-output field relationship, identify the bistability regions, and examine the "phase switching" effect in both the absorptive and dispersive cases, thus extending and complementing the results of [12–14]. The second part of the paper is concerned with the stability analysis and the chaotic behaviour of the system mentioned.

2 The model equations

We consider a single-mode ring cavity (Fig. 1) which contains an atomic medium of length L, with an input field $E_{\rm I}$ at the mirror M_1, a squeezed vacuum field is introduced at the mirror M_2 and the transmitted field is $E_{\rm T}$. The two mirrors M_1 and M_2 have reflectivity R and transmitivity $T\,(=1-R)$ while the mirrors M_3 and M_4 have 100% reflectivity. The total length of the cavity is $\mathcal{L}=2(\ell+L)$ and z is the position within the atomic medium. The boundary conditions (BC) for the single-mode (c-number) cavity field $E(z,t)$ at $Z=0,L$ are of the form [16]

$$E(0,t)=\sqrt{T}E_{\rm I}(t)+RE(L,t-\Delta t)\exp(-{\rm i}\theta T) \quad (1a)$$

$$E(L,t)=E_{\rm T}(t)/\sqrt{T}. \quad (1b)$$

Here $\Delta t=(2\ell+L)/c$, is the time for light to travel from M_2 to M_1, c is the velocity of light in vacua, $\theta=(\omega_{\rm c}-\omega_{\rm d})/(c/\mathcal{L})$ is the normalised cavity detuning parameter, $\omega_{\rm c}$ is the frequency of the cavity mode and $\omega_{\rm d}$ is the frequency of the incident field. The decay rate for the cavity is defined by $k=c/\mathcal{L}$.

The atomic medium is composed of a system of homogeneously broadened 2-level atoms of transition frequency ω_o and atomic density n_o. As stated previously the atoms are coupled to the single-mode cavity field and to the squeezed vacuum field where the introduction of both fields at different ports means we can ignore the coupling between them. Starting from a Hamiltonian model that describe the above interaction it is shown that (Appendix A) the model equations of motion for the *mean values* of the cavity field $\alpha\equiv E(z,t)$, the atomic polarization components $J_{\pm}(z,t)$ and the atomic population $J_z(z,t)$ are expressed by the c-number Maxwell-Bloch equations,

$$\frac{\partial\alpha}{\partial t}+c\frac{\partial\alpha}{\partial z}=-gn_oJ_- \quad (2a)$$

$$\frac{\partial J_-}{\partial t}=-GJ_-+2g\alpha J_z-\gamma MJ_+=\left(\frac{\partial J_+}{\partial t}\right)^* \quad (2b)$$

$$\frac{\partial J_z}{\partial t}=-\gamma_{\parallel}J_z-\frac{1}{2}\gamma-g(\alpha J_++\alpha^*J_-). \quad (2c)$$

The notations are: γ is the A-coefficient, $\gamma_{\parallel}=\gamma(1+2N)$, $G=(1/2)\gamma_{\parallel}+{\rm i}\gamma\delta$ where $\delta=(\omega_o-\omega_{\rm d})/(\gamma/2)$ is the normalised atomic detuning and g is the coupling constant between the atoms and the cavity field. The squeezed vacuum field parameters are N and M with $|M|^2\le N(N+1)$: N being the average photon number of the squeezed field at the atomic resonance frequency ω_o, and M is the measure of the correlations between pairs of photons (see appendices for their definitions in terms of the creation and annihilation field operators). For simplicity we will assume perfect squeezing, so that $|M|=\sqrt{N(N+1)}$.

In this paper (Part I) we are concerned with the steady behaviour of the model equations (2) with the boundary conditions (1). In the steady state, where the time derivatives in equations (2) are set to zero, and by integrating equations (2a) w.r. to z and using the BC of equations (1) we get the following equation,

$$y=x(1+{\rm i}\theta)+C\bar{J}_-, \quad (3)$$

where $y=2g\sqrt{T}E_{\rm I}/\gamma$ and $x=2g\sqrt{T}E_{\rm T}/\gamma$ are the normalised input and output field amplitudes respectively and $C=2\sqrt{2}g^2n_o/(\gamma k)$ is the cooperative parameter (without loss of generality, y is taken to be real). Note that to reach equation (3) we have used that $\mathrm{e}^{-{\rm i}\theta T}\approx 1-{\rm i}\theta T$ for $T\ll 1$. Within the (spatial) mean field limit [16], valid for $T\ll 1$, we set $\overline{\alpha J}_{\pm,z}\approx\overline{\alpha}\overline{J}_{\pm,z}$ where $\overline{J_-}=L^{-1}\int_0^L J_-(z){\rm d}z$, etc., define spatial average quantities, the steady state solutions of equations (2b, 2c) for the atomic variables are given by

$$\overline{J}_z=\frac{-1}{2(1+2N)}(1+\delta^2)\left[1+\delta^2+b_1|x|^2\right]^{-1} \quad (4)$$

$$\overline{J}_-=\frac{-1}{\sqrt{2}}x(b_1-{\rm i}b_2)\left[1+\delta^2+b_1|x|^2\right]^{-1} \quad (5)$$

where

$$b_1=1-\frac{2|M|}{1+2N}\cos\phi,$$
$$b_2=\frac{\delta+2|M|\sin\phi}{1+2N}\,. \quad (6)$$

Here $\phi=\phi_{\rm s}-2\phi_{\rm f}$ is the relative phase of the squeezed vacuum field, where $\alpha=|\alpha|\exp({\rm i}\phi_{\rm f})$. With (5) substituted into (3) we get the characteristic input-output field amplitudes relation,

$$y=x\left[1+{\rm i}\theta+2C\frac{b_1-{\rm i}b_2}{1+\delta^2+b_1|x|^2}\right]. \quad (7)$$

In the normal vacuum case ($N=M=0$) equation (7) reduces to the relation $y=x[1+\ 2C/(1+|x|^2)]$ in the absorptive case ($\theta=\delta=0$) [17], while in the dispersive case ($\theta,\ \delta\neq 0$) equation (7) reduces to the relation $y=x[1+{\rm i}\theta+2C(1-{\rm i}\delta)/(1+\delta^2+|x|^2)]$ [18,19]. Also, the relation (7) is identical to the relation derived, within the mean field limit, for a Fabry-Perot (FP) cavity configuration [20] using Fleck's type of harmonic truncation for treating the standing wave effects [21] (a different type of treatment for the standing wave effects

in a FP cavity, like McCall's type of spatial average [22], gives a "quantitatively" different state input-output relation [20]).

The conditions for the bistable behaviour according to equation (7) with (N, $M \neq 0$) are analysed next.

3 Conditions for bistability

Equation (7) gives the steady-state intensity transmission function,

$$Y = \frac{X}{(1+\delta^2+b_1X)^2}\left[(1+\delta^2+b_1(X+2C))^2 + (\theta(1+\delta^2+b_1X)-2Cb_2)^2\right] \quad (8)$$

where $Y = y^2$ and $X = |x|^2$ are the transmitted and input field intensities respectively.

The input intensity Y has a qualitatively different shape for values of C above or below a critical value of C. Below this critical value of C, Y is a monotonic function of X so that X is a single-valued function of Y. Above this critical value of C, Y has a maximum and a minimum separated by a point of inflexion, at which $\mathrm{d}^2Y/\mathrm{d}X^2 = 0$, and where

$$X_{\mathrm{inf}} = D_2\frac{D_2(1-\theta D_1)+2C(1+D_1^2)}{D_2(\theta D_1-1)+C(1+D_1^2)}, \quad (9)$$

with $D_1 = b_2/b_1$, $D_2 = D_o/b_1$ and $D_o = 1+\delta^2$.

In this case X is multivalued so that with a suitable selection of the parameters of the system the steady-state transmission plot of $|x|$ as a function of y has the typical bistable curve.

The conditions for bistability are [19]

$$X_{\mathrm{inf}} > 0 \quad (10a)$$

and

$$\left(\frac{\mathrm{d}Y}{\mathrm{d}X}\right)_{X_{\mathrm{inf}}} < 0 \quad (10b)$$

where X_{inf} is given by (9). The first condition ensures the inflexion point is within the physical region for which $X \geq 0$. The second condition ensures that the curve of Y against X has a maximum and a minimum. It identifies the values of the parameters for which optical bistability is possible. According to (9), the second condition requires that $f(\theta,\delta) > 0$ where

$$f(\theta,\delta) = [2C(1+D_1^2)+2D_2(\theta D_1-1)]^3 - 54CD_2^2(1+D_1^2)^2(1+\theta^2), \quad (11)$$

3.1 Absorptive case

When the atomic and cavity frequencies are equal to the frequency of the driving field, that is, $\delta = \theta = 0$, condition (10b) gives the critical value of C, C_{crit}, at which $f(\delta,\theta) = f(0,0) = 0$, *i.e.*

$$[2C_{\mathrm{crit}}(1+D_1^2)-2D_2]^3 - 54C_{\mathrm{crit}}D_2^2(1+D_1^2)^2 = 0. \quad (12)$$

The positive real root of (12) in conformity with (10a) is found to be:

$$C_{\mathrm{crit}} = \frac{D_2}{1+D_1^2}\left[1+3\sqrt{1+D_1^2}\cos\left(\frac{1}{3}\tan^{-1}(D_1)\right)\right]. \quad (13)$$

In the normal vacuum ($N = |M| = 0$) $C_{\mathrm{crit}} = 4$, as first shown by Bonifacio and Lugiato [17]. Otherwise C_{crit} has period 2π and is symmetric about $\phi = \pi$ so comments will be restricted to the interval $0 \leq \phi \leq \pi$. The plot of C_{crit}, equation (13), as a function of N and ϕ is shown in Figure 2a.

For *fixed* N, C_{crit} has minimum and maximum values at $\phi = \pi, 0$ respectively given by

$$C_{\mathrm{crit}}^{\mathrm{min}} = 4/\left(1+\frac{2\sqrt{1+2N}}{1+2N}\right) < 4 \quad (14)$$

$$C_{\mathrm{crit}}^{\mathrm{max}} = 4(1+2N)(1+2N+2\sqrt{N(N+1)}) > 4. \quad (15)$$

Equation (14) means that in the absorptive case the threshold for bistability in the squeezed vacuum case is less than the threshold in the normal vacuum case (*cf.* [15] and comments in the summary, Sect. 5).

For $N \gg 1$, $C_{\mathrm{crit}}^{\mathrm{max}} \to 32N^2$ and $C_{\mathrm{crit}}^{\mathrm{min}} \to 2$, the smallest possible value of C_{crit}. In the limit $N \to \infty$ and arbitrary ϕ, equation (13) gives

$$(C_{\mathrm{crit}})_{N\to\infty} = \frac{3\cos((\pi-\phi)/6)}{2\sin(\phi/2)} + \frac{1}{2}\,. \quad (16)$$

This is a monotonic decreasing function of ϕ with a singularity at $\phi = 0$. Numerically, $(C_{\mathrm{crit}})_{N\to\infty} = 4$ at $\phi \approx 46.75°$. In Figure 2b the plot of the expression (13) for C_{crit} against ϕ shows that near $\phi = 0$, C_{crit} increases more rapidly as N increases. Figure 2c shows the behaviour of C_{crit} *versus* N for various values of ϕ. If $\pi/2 \leq \phi \leq \pi$, $C_{\mathrm{crit}} = 4$ at $N = 0$ and decreases monotonically to a value < 4, given by equation (16). If $0 \leq \phi < \pi/2$, C_{crit} monotonically increases to a maximum before decreasing monotonically to a value given by equation (16). This analysis shows that when the atomic medium is coupled to squeezed light and the phase of the squeezed light satisfies the inequality $\pi/2 \leq \phi \leq \pi$ the critical value of the cooperative parameter C is always reduced below that required in the ordinary vacuum but if $0 \leq \phi \leq 46.75°$, C_{crit} is always greater than 4.

Finally in this section a few comments are made about the input-output relationship of equation (8). The two cases where $\phi = 0$ and $\phi = \pi$ are of special interest for then $b_2 = 0$ and $b_1 = 1 \mp 2|M|/(1+2N)$ and so equation (8) reduces to

$$Y = X\left(1+\frac{2b_1C}{1+b_1X}\right)^2. \quad (17)$$

Using the transformation $Y_1 = b_1Y$, $X_1 = b_1X$ and $C_1 = b_1C$, equation (17) takes the familiar form for the input-output relation for absorptive optical bistability in the

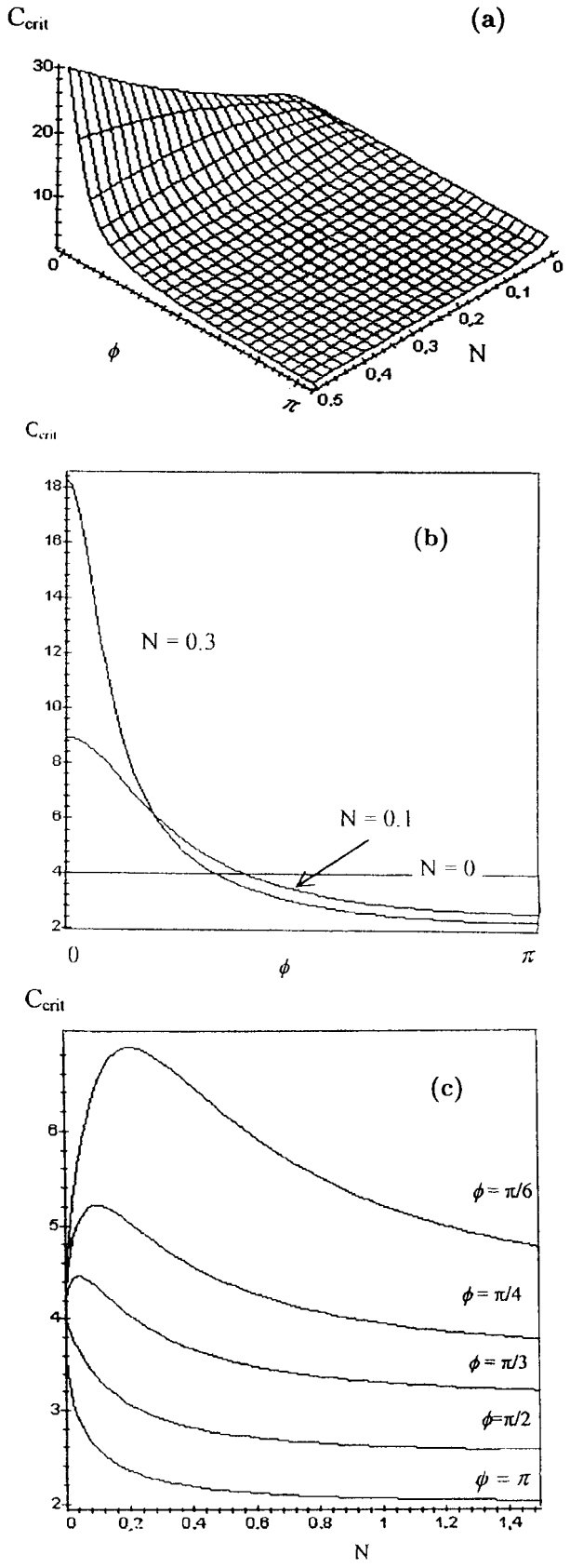

Fig. 2. (a) A 3-dimensional plot of $C_{\rm crit}$ as a function of ϕ and N. (b) $C_{\rm crit}$ *versus* ϕ for $N = 0$ (normal vacuum), 0.1 and 0.3. (c) $C_{\rm crit}$ *versus* N for various values of ϕ.

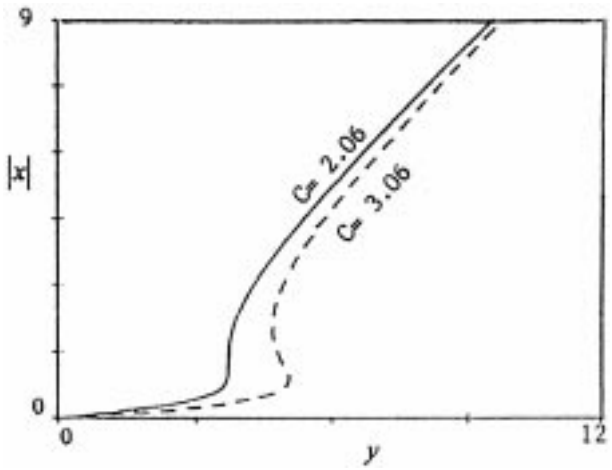

Fig. 3. The transmitted field $|x|$ *versus* the driving field y, for $N = 1$, $\phi = \pi$ and different values of C.

normal vacuum [17], namely,

$$Y_1 = X_1 \left(1 + \frac{2C_1}{1 + X_1}\right)^2. \tag{18}$$

Note that Y_1, X_1 and C_1 are functions of N. Specifically,

$$C_1 = C\left(1 \mp \frac{2\sqrt{N(N+1)}}{1+2N}\right) \tag{19}$$

for $\phi = 0$, π respectively. According to (18) the critical value of C_1 is 4 [17]. Hence, in the squeezed vacuum case and in the absorptive case, with N fixed the critical value of C for $\phi = 0$ is greater than that for $\phi = \pi$. Figure 3 plots $|x|$ against y for $N = 1$ and $\phi = \pi$ which shows the critical case for bistability, $C = 2.06$, and a typical bistable curve for $C = 3.06$. For these values of C and N optical bistability is not physically possible if $\phi = 0$.

3.2 Dispersive case

In this case either or both the atomic detuning δ and the cavity detuning θ are non-zero. By choosing certain values of the parameters C and N the condition $f(\delta, \theta) = 0$, equation (10b), together with the restriction $X_{\rm inf} > 0$, equation (10a), defines a region in the parameter space (f, δ, θ) within which optical bistability can be found. The regions were obtained by plotting the contour $f(\delta, \theta) = 0$ in the (δ, θ) plane. Next we comment on the general behaviour of these contours.

For values of $C \gg 1$ and small N it can be shown that (see Appendix B) when $|\theta| \gg 1$, $|\delta| \gg 1$ the boundary of the bistability region is approximated by one of the two hyperbolas

$$\theta(\delta - \delta_o) = \frac{-C}{4(1+2N)},$$
$$\theta(\delta - \delta_o) = \frac{2C}{(1+2N)} \tag{20}$$

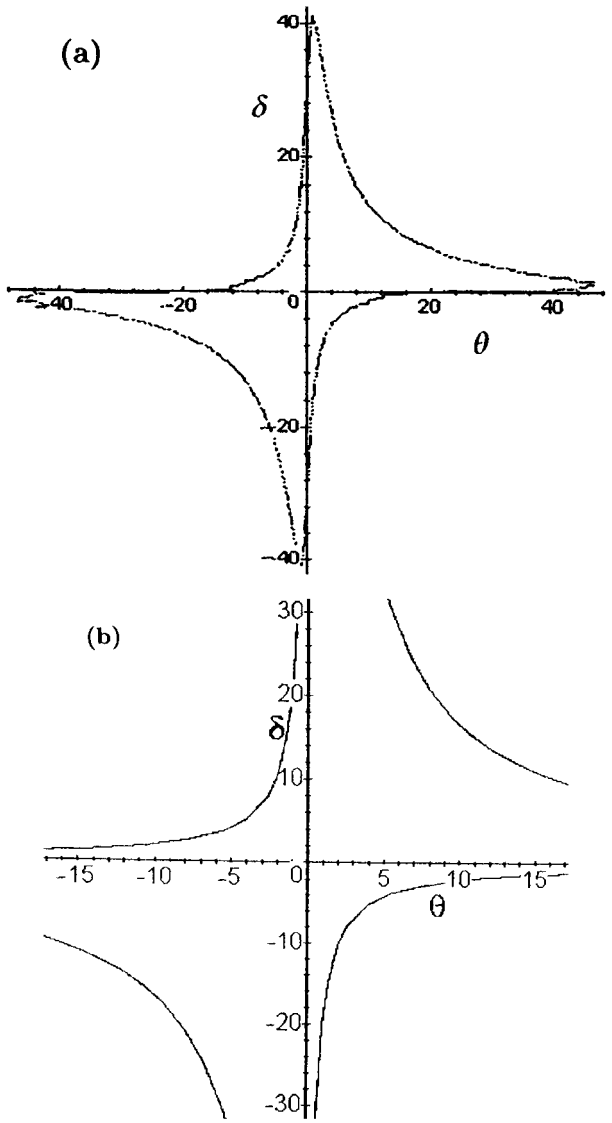

Fig. 4. (a) The contour surrounding the bistable region for $C = 100$, $N = 0.1$ and $\phi = 0$. (b)The asymptotic contours (of Eq. (20)).

where $\delta_o = 2|M| \sin\phi$. Further, this boundary crosses the θ-axis at the two points,

$$(\delta^{\pm})_{\theta=0} = 2|M| \sin\phi \pm C\sqrt{\frac{4}{27}}(1+2N)^{-1} \qquad (21)$$

and crosses the line $\delta = -\delta_o$ at the points

$$(\theta^{\pm})_{\delta=-\delta_o} = \pm C\sqrt{\frac{4}{27}}\frac{\left(1 - \dfrac{2|M|}{1+2N}\cos(\phi)\right)}{1+\delta_o^2}\,. \qquad (22)$$

Figure 4 show the contours for $C = 100$, $N = 0.1$ and $\phi = 0$: Figure 4a plots the exact (numerical) contour, while Figure 4b plots the asymptotic contours of equation (20), valid for $|\theta|, |\delta| \gg 1$, and drawn between $(\delta^{\pm})_{\theta=0}$ and $(\theta^{\pm})_{\delta=-\delta_o}$.

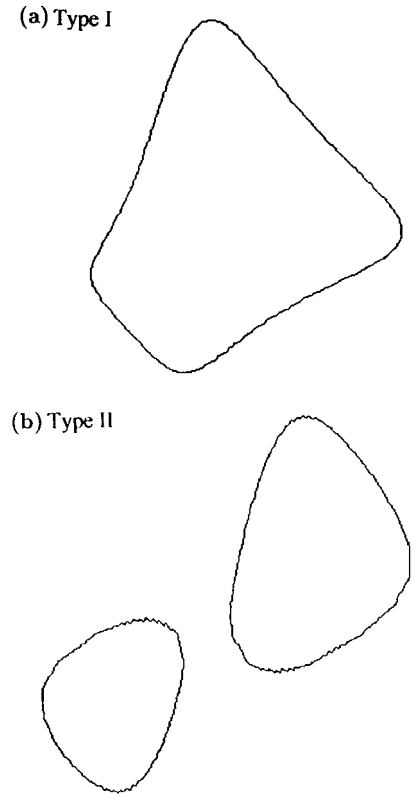

Fig. 5. The two topologically distinct bistability regions in the (δ, θ) plane.

The remaining comments in this section are based upon the results of extensive numerical experiments supplemented by the analysis of optical bistability in the absorptive case. Our finding is that the region of optical bistability is either enclosed by one or two disconnected simple closed curves. These two topologically distinct cases are shown in Figure 5. If the region of bistability is enclosed by a single simple contour as in Figure 5a we will call this a type I region. We call the other topologically distinct region shown in Figure 5b a type II region: in this case the two contours are centered in the first and third quadrant of the (δ, θ) plane. We will show a sample of contours with N fixed but C and ϕ are varied. A good guide to predicting the behaviour of the region of bistability in the dispersive case is provided by the above analysis in the absorptive case especially the plots of Figure 2b, showing the behaviour of $C_{\rm crit}$ against ϕ for different values of N. Figure 6 shows one of these curves for $N = 0.1$ cut by several horizontal lines where each line corresponds to a fixed value of C. These lines can either: lie above $C_{\rm crit}^{\rm max}$ (the maximum critical value of C), see line (i) in Figure 6; cut the graph of $C_{\rm crit}$ at a point close to but just below $C_{\rm crit}^{\rm max}$, as in line (ii) in Figure 6; or cut the graph well below $C_{\rm crit}^{\rm max}$ as in line (iii) in Figure 6. Next, we consider the behaviour of the bistability region as ϕ and C vary using this Figure 6 as a guide.

For C fixed at a value greater than $C_{\rm crit}^{\rm max}$, represented by the line (i) in Figure 6, the bistability region is a type I region enclosing the origin for all value of ϕ. For example

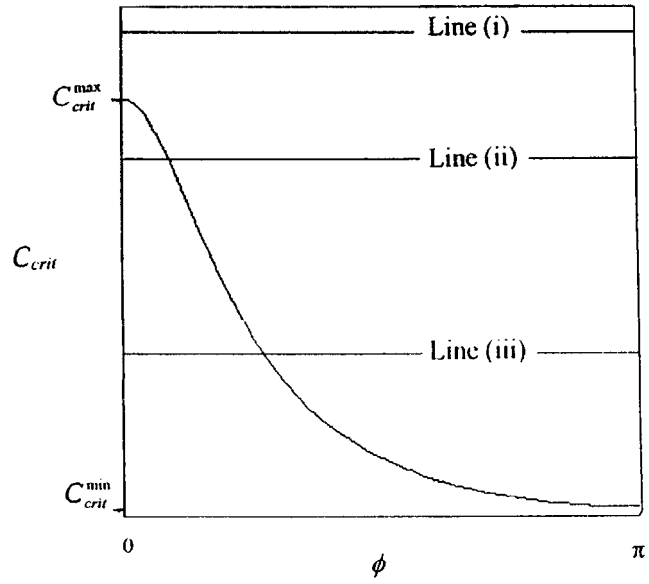

Fig. 6. $C_{\rm crit}$ *versus* ϕ for $N = 0.1$ ($C_{\rm crit}^{\rm max} = 8.944$, $C_{\rm crit}^{\rm min} = 2.576$).

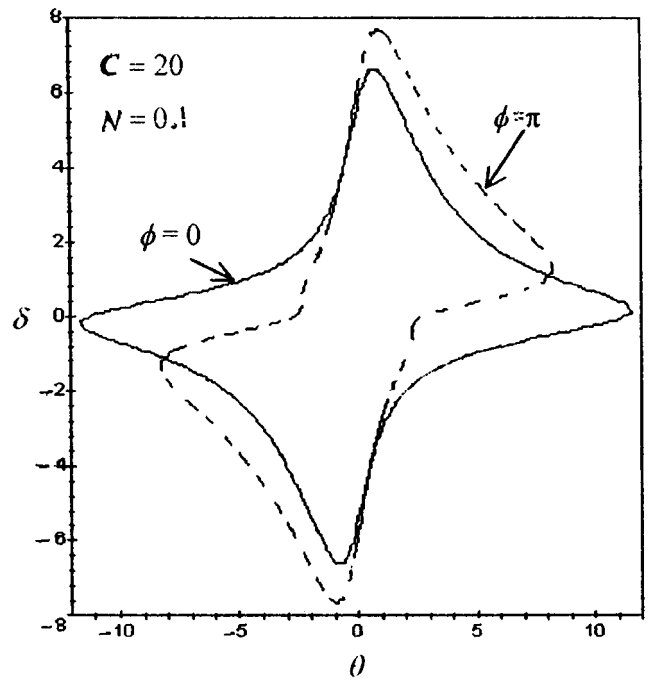

Fig. 7. The bistability region with $C = 20$ and $N = 0.1$ for $\phi = 0$ and $\phi = \pi$.

Figure 7 shows the behaviour of the bistability region with $C = 20$ with $N = 0.1$ for $\phi = 0$ and $\phi = \pi$. The bistability region for values of ϕ in between these values are very similar and, as predicted in the absorptive case, always enclose the region. As C decreases the bistability remains of type I region until for a value of $C < C_{\rm crit}^{\rm max}$ this region splits into a type II region. As C decreases further the region of bistability at $\phi = 0$ remains of a type I region but as ϕ increases this type I region changes into a type II region. Figure 8 shows the bistability regions for $C = 8$ and

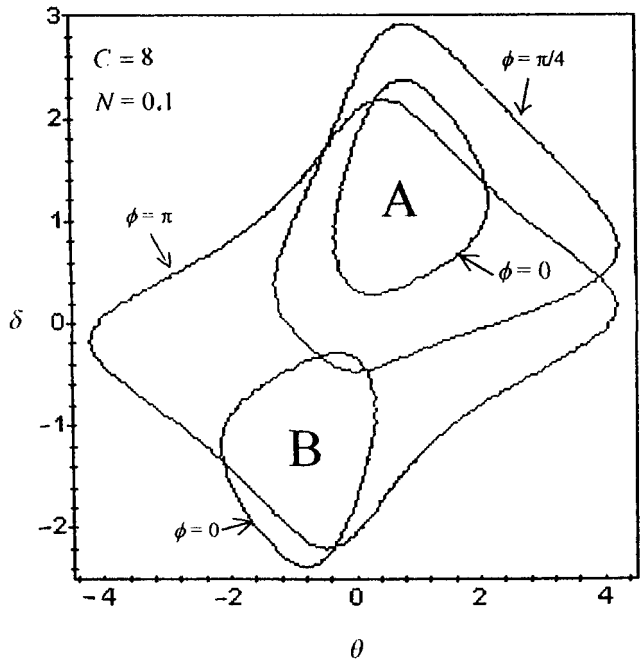

Fig. 8. The bistability regions for $C = 8$ and $N = 0.1$ for $\phi = 0, \pi/4$ and π.

$N = 0.1$ for $\phi = 0, \pi/4$ and π (the value of $C = 8$ is represented by the line (ii) of Fig. 6): at $\phi = 0$ the bistability region is enclosed by two separate simple closed contours. As ϕ increases region A grows and region B shrinks until at $\phi \approx 0.3889$ rad it disappears. For $\phi > 0.3899$ rad the bistability region encloses the origin, in agreement with the results in the absorptive case. The size of the bistability region grows as ϕ increases and moves more into the third quadrant of the (δ, θ) plane and the region becoming more symmetrically placed about the line $\delta = \theta$ as $\phi \to \pi$.

Eventually as C decreases the type I region disappears but a type II bistability region remains for some interval $\phi_1 \leq \phi \leq \pi$. As C decreases further ϕ_1 decreases until $C = C_{\rm crit}^{\rm min}$ there is no region of bistability: $C_{\rm crit}^{\rm min}$ is the minimum value of $C_{\rm crit}$. Figure 9 shows the bistability regions for $C = 5$ and $N = 0.1$ for $\phi = \pi/6, \pi/4, \pi/2$ and π (this value of C is represented by line (iii) of Fig. 6). For $0 \leq \phi \leq 0.3420$ rad there is no region of bistability. For $\phi > 0.3420$ rad the region of bistability is a single closed region. For $\phi \approx 0.8407$ rad this region encloses the region. The size of the bistability region grows as ϕ increases and moves more into the third quadrant of the $\delta - \theta$ plane and becomes more symmetrical about the line $\delta = \theta$ as $\phi \to \pi$.

Finally, for $C = 4$ (the critical value of C in the normal vacuum for the absorptive case [17]) and for $\phi = 0$ there is no region of bistability in the (δ, θ) plane. But for $\pi/4 \leq \phi \leq \pi$ and arbitrary N, there is a region of bistability-unlike the normal vacuum case [18,19]. In this case the bistable contour includes the origin and expands as N increases rapidly converging to the contour for the case $N \to \infty$ (Fig. 10).

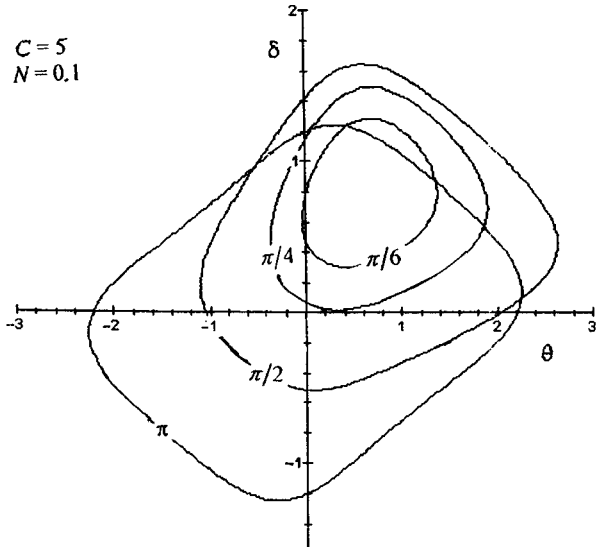

Fig. 9. The bistability regions for $C = 5$ and $N = 0.1$ and various values of ϕ.

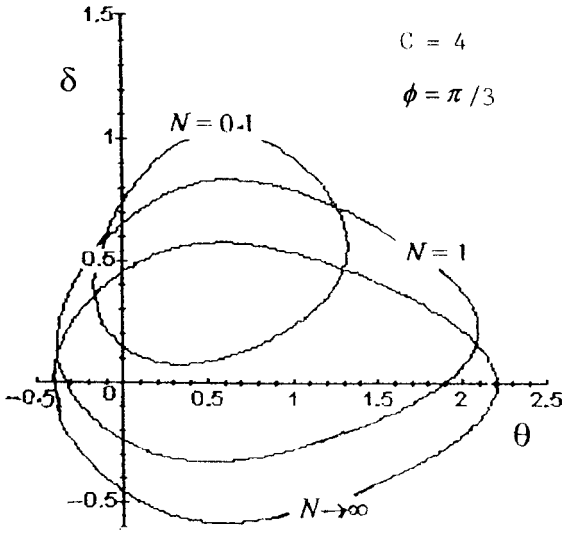

Fig. 10. The bistability regions for $C = 4$, $\phi = \pi/3$ and various values of N.

4 Phase switching effects: isolas and mushrooms

When the coherent input field Y is kept fixed the authors of [14] have shown that in the dispersive case the output field can switch from the lower to the higher transmission state and *vice versa* by varying the phase of the squeezed vacuum. Here we examine in detail the same and similar effects in both absorptive and dispersive OB.

4.1 Absorptive case

For convenience, the contour plots showing the variation of $|x|$ with ϕ will be referred to as switching diagrams. As ϕ varies the system can switch between two different physical states. Our numerical experiments show that the possible switching behaviour depends on whether $C \gtrless C_{\rm crit}^{\rm max}$.

First, we present results for $C = 20$, $N = 0.1$. In this case $C > C_{\rm crit}^{\rm max}$. Figure 11a shows the 3-dimensional plot, using equation (8), of the driving field y as a function of the transmitted field $|x|$ and the phase ϕ, in the absorptive case ($\theta = 0$, $\delta = 0$). The contours of this plot at the fixed values of the input $y = 13$ and 18 are given in Figures 11c and 11d showing an *isola* structure for the dependence of the output field on the squeeze phase parameter ϕ. The switching diagrams in Figure 11c was obtained by fixing the input field at $|y| = 13$ in the region of the local minimum (Fig. 11a). In this case at $\phi = 0$ the output field $|x|$ has the values corresponding to either of the points P_1 and P_2 marked on the input-output curve of Figure 11b. P_1 is on the *upper* branch of the OB curve and P_2 on its *lower* branch. Figure 11c shows how these points move as ϕ varies. As ϕ increases P_1 moves along curve I in Figure 11c staying on the stable upper branch of an OB curve until it reaches the point labeled A. Here the system becomes unstable and P_1 jumps to the stable lower branch of the OB curve. As ϕ increases further P_1 remains on a stable lower branch of the input-output curves moving along the curve labeled II in Figure 11c. The movement of the point P_2 as ϕ increases is simple: it remains on the stable lower branch of an OB curve moving smoothly along curve II of Figure 11c. Note that there is only the possibility of one-way switching, a switch-down from curve I to curve II, since if the system is on curve II it will stay on this curve for any variation of ϕ.

However, for a larger fixed input value y, close to the local maximum value of y, one-way switching from the lower branch to the upper branch is possible. This is demonstrated in Figures 11b and 11d for $y = 18$. At $\phi = \pi/2$ the output field $|x|$ can again take either of two values corresponding to the point P_1' on the upper branch of the OB curve in Figure 11b and P_2' on the lower branch. As ϕ varies monotonically P_2' moves along the lower curve in Figure 11d, staying on the stable branch of an OB curve until the system becomes unstable and switches up to the upper branch in Figure 11d. For the other possibility, corresponding to the point P_1' on the upper curve of Figure 11d, the output field $|x|$ is almost unchanged for any variation of ϕ. This behaviour means that in this absorptive case only one-way switching is possible, either switching up, as in Figure 11d or down as in Figure 11c. Other switching behaviour is possible in the absorptive case. Generally, switching will occur at values of y close to the local maximum or minimum of the 3-dimensional plot of y as a function of $|x|$ and ϕ where both N and C are kept fixed.

So far, we have considered the case of $C > C_{\rm crit}^{\rm max}$ where optical bistability is possible for all values of ϕ and the switching behaviour is of the form shown in Figures 11c and 11d. However if $C < C_{\rm crit}^{\rm max}$ the switching behaviour shown in Figure 11c is not possible since the analysis in the absorptive case shows that there is no optical bistability if $0 \leq \phi \leq \phi_1$, where ϕ_1 depends on the value of C

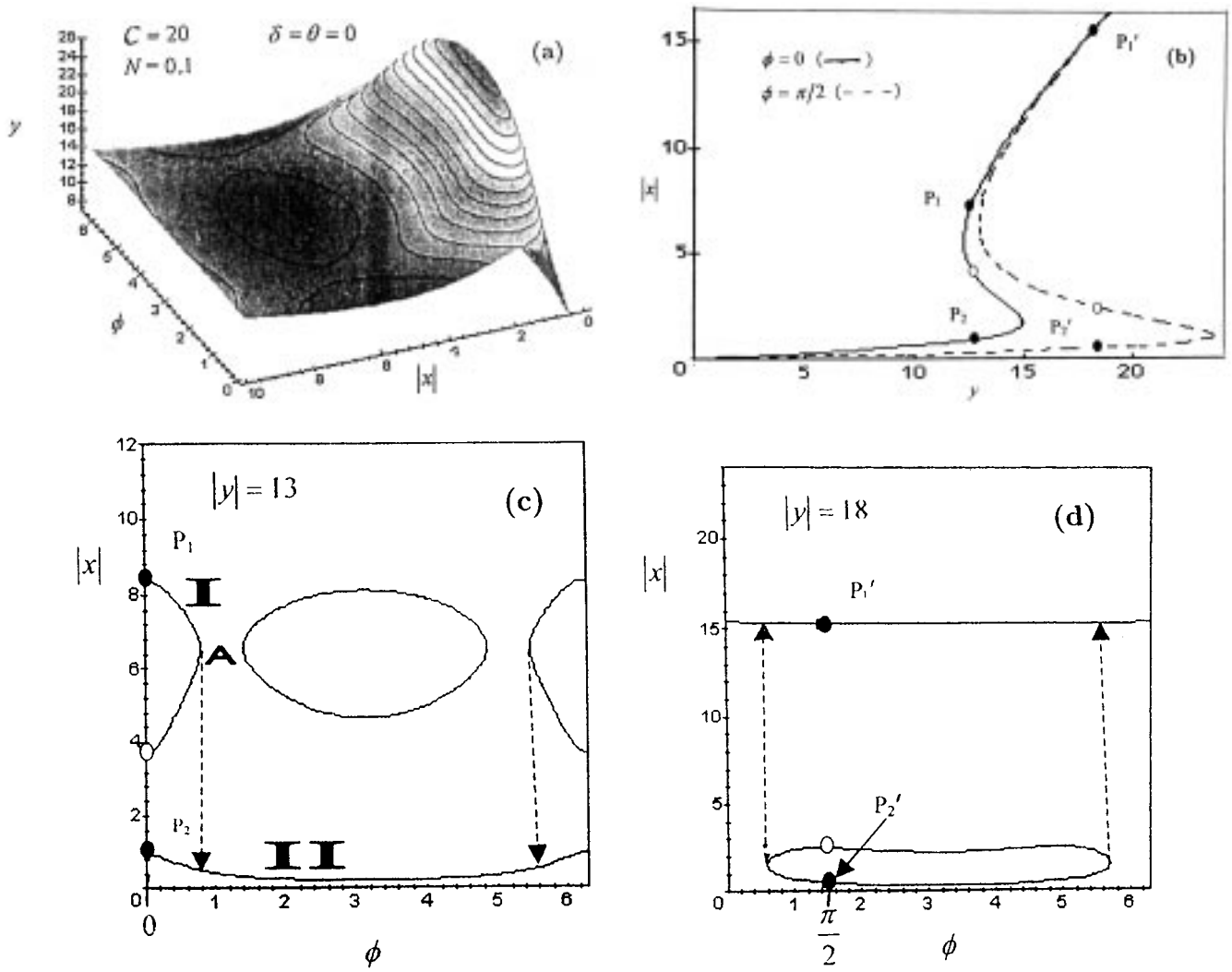

Fig. 11. (a) The driving field y *versus* the transmitted field $|x|$ and ϕ in the absorptive case. (b) The transmitted field $|x|$ *versus* the driving field y for $\phi = 0, \pi/2$. (c) The switching diagram: $|x|$ against ϕ at $y = 13$ (isola structure). (d) As (c) but for $y = 18$.

and N. For example, if $C = 8$ and $N = 0.1$, $C < C_{\text{crit}}^{\max}$ so the switching behaviour of Figure 11d is impossible. However, other switching behaviour is possible. For these values of C and N, Figure 12 shows the 3-dimensional plot of y against $|x|$ and ϕ. If the input is fixed at $y = 7.8$ and at $y = 8$ the switching diagrams are shown in Figures 12b and 12c. Both figures indicate two-way switching. In Figure 12b, at $\phi = 0$ the output field $|x|$ corresponds to a single point Q on the stable upper branch of an OB curve. As ϕ increases Q moves continuously along the upper part of the curve in Figure 12b, until at the point A the system becomes unstable. Then Q jumps to the stable lower branch of an OB curve, moving along the lower part of the curve in Figure 12b. As ϕ increases further Q moves on the lower part of the curve until at B the system becomes unstable again so the point jumps from the lower curve to the upper curve. If y is increased slightly to 8, Figure 12c shows the switching behaviour of the system. Compared to Figure 12b the new feature is the closed contour symmetrically placed around $\phi = \pi$. If initially the state of the system is represented by a point on the upper part of this closed contour, for example at R, the system is on the upper stable branch of an OB curve. As ϕ changes monotonically this point will move along this contour until at either the point C or D the system becomes unstable so that the point jumps to the lower curve I in Figure 12c.

4.2 Dispersive case

In this case, where δ, $\theta \neq 0$, the switching diagram still show some of the features seen in the absorptive case. For example, Figure 13 shows the switching diagram for $C = 20$, $N = 0.1$, $\delta = 0.1$ and $\theta = 0.1$. It is very similar to the switching diagram of Figure 12b except that it is not symmetrical about $\phi = \pi$. Extra feature is seen in Figure 14 where the switching diagram shows a *mushroom*-shape structure so that two-way switching is possible-as first reported in [14]. Here the points S and T on the

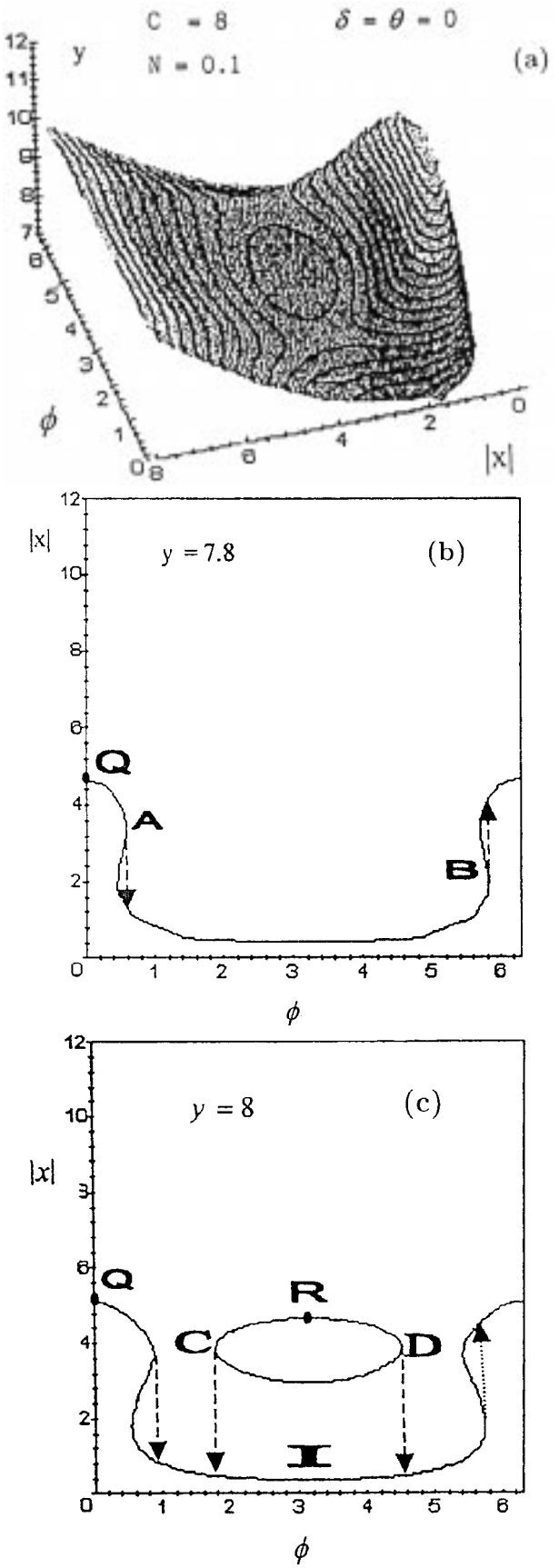

Fig. 12. (a) As in Figure 11a but for $C = 8$. (b) The switching diagram at $y = 7.8$. (c) As (b) but for $y = 8$.

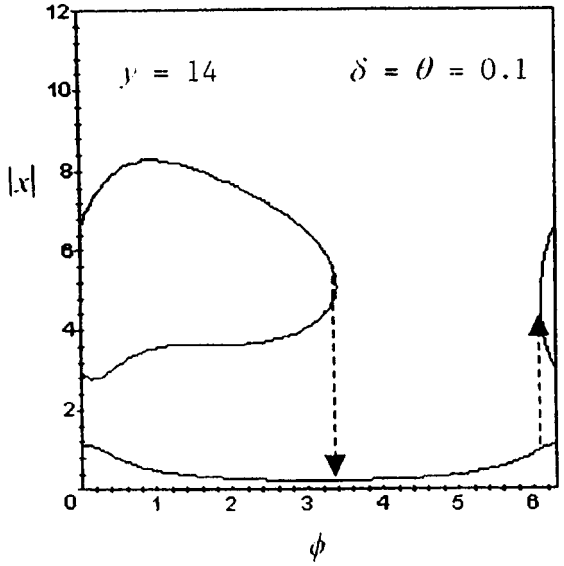

Fig. 13. Switching diagram for $C = 20$, $N = 0.1$ in the dispersive case (asymmetric isola structure).

switching diagram of Figure 14c correspond to the points S and T on the input-output diagram for $|\phi| = 2.0$ rad of Figure 14b. As ϕ increases the point T moves along the lower part of the mushroom-shaped curve in Figure 14c until at the point A the system becomes unstable and jumps to the point A′ on the upper part of the curve. As ϕ increases further the system moves along the upper part of the mushroom curve until it again becomes unstable and jumps down at B to the stable state represented by the point B′ in Figure 14c. We have checked that by numerical experiments that this type of switching behaviour is possible for most systems with $C \gg 1$, $\delta > 1$ and $\theta \ll 1$.

5 Summary

We have presented a steady state analysis of the effects induced by a squeezed vacuum field on optical bistability in a ring cavity. Based on a set of Maxwell-Bloch equations *derived* (Appendix A) for a system of 2-level atoms within the usual Born, Markov and rotating wave approximations, our investigation is presented within the (spatial) mean field limit. In the absorptive case the smallest possible critical value of the cooperative parameter $C_{\rm crit}^{\rm min}$ is 2 for (relative) squeeze phase $\phi = \pi$ in comparison with the value $C_{\rm crit} = 4$ in the normal vacuum case [17]. In general, for $\pi/2 < \phi \leq \pi$, $C_{\rm crit} < 4$ but for $0 < \phi \lesssim 46.5°$, $C_{\rm crit} > 4$. In the dispersive case, where both the atomic and cavity detuning $(\delta, \theta) \neq 0$, the region of bistability in the (δ, θ) plane are identified analytically for $C \gg 1$ and for $|\delta|, |\theta| \geq 1$. Our extensive numerical investigation, and in conformity with the analytical results for the absorptive case, shows that the bistable region in the (δ, θ) plane is either one or two disconnected simple closed curves, depending on the values of $C > C_{\rm crit}^{\rm max}$, C just below $C_{\rm crit}^{\rm max}$ and $C \ll C_{\rm crit}^{\rm max}$, ($C_{\rm crit}^{\rm max}$ is the maximum possible value of $C_{\rm crit}$).

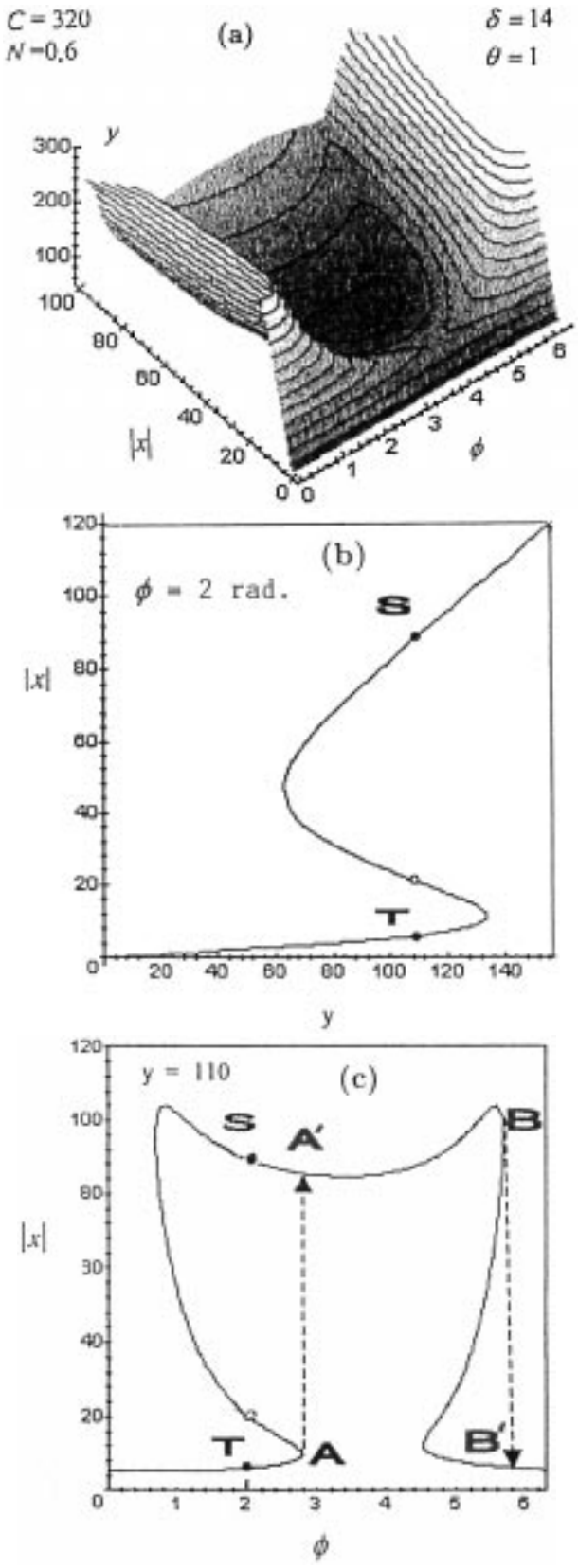

Fig. 14. (a) As Figure 11a but in the dispersive case. (b) The transmitted field $|x|$ *versus* the driving field y for $\phi = 2$ rad. (c) The switching diagram, $|x|$ against ϕ (mushroom structure).

We have also investigated the utilization of the phase of the squeezed field to switch the system between a high and a low transmission state. Our numerical and theoretical investigations show that in the absorptive case both one-way and two-way switching is possible. The type of switching depends on whether the cooperative parameter $C \lessgtr C_{\rm crit}^{\rm max}$. If $C > C_{\rm crit}^{\rm max}$ the one-way switching behaviour (isola structure) of Figures 11c and 11d is possible. If $C < C_{\rm crit}^{\rm max}$ the-two way switching behaviour of Figures 12b and 12c is observed. In the dispersive case a two-way switching behaviour is observed in the form of an asymmetrical isola structure, Figure 13, or in the form of mushroom-type structure [14], Figure 14c. The steady state behaviour of the isola and mushroom structure exhibited here resembles that which occurs in some real biological reactions [23].

In the following paper (Part II), we investigate the dynamical behaviour of the model Maxwell-Bloch equations, equations (2), concerning stability, self-pulsing and chaotic behaviour.

Appendix A

Here we present a derivation of the model Maxwell-Bloch equations, equations (2). We begin with the Hamiltonian form for an extended system of N_a homogeneously broadened 2-level atoms of transition frequency ω_o coupled to the quantised radiation field in electric dipole approximation [24]

$$H = H_o + H_1 \tag{A.1}$$

where

$$H_o = \sum_{\underline{k},\lambda} \hbar\omega_k a^\dagger_{\underline{k},\lambda} a_{\underline{k},\lambda} + \frac{1}{2}\hbar\omega_o \int_V \sigma_z(\underline{x},t)\mathrm{d}\underline{x}, \tag{A.2}$$

is the Hamiltonian of the unperturbed system of field and atoms,

$$H_1 = -\int_V \underline{p}(\underline{x},t).\mathbf{e}(\underline{x},t)\mathrm{d}\underline{x}. \tag{A.3}$$

is the interaction Hamiltonian. The atomic operator densities are

$$\sigma_z(\underline{x},t) = \sum_{i=1}^{N_a} \sigma_z^i(t)\delta(\underline{x}-\underline{x}_i)$$
$$\underline{p}(\underline{x},t) = p\underline{\hat{u}} \sum_{i=1}^{N_a} \sigma_x^i(t)\delta(\underline{x}-\underline{x}_i) \tag{A.4}$$

where $\underline{x}_i$ is the site of atom i and $\underline{x}_i \in V$ (the volume of the macroscopic region, *i.e.* the cavity), p is the magnitude of the atomic dipole matrix element and $\underline{\hat{u}}$ is a unit vector in the direction of $\underline{p}$. The operators $(\sigma_x^i, \sigma_y^i, \sigma_z^i) = \boldsymbol{\sigma}^i$ are the spin-(1/2) Pauli matrices for each atom labelled i,

and each satisfies an su(2) Lie algebra – which means that the operator densities satisfy the commutation relations

$$[\sigma_x(\underline{x},t),\sigma_y(\underline{x}',t)] = 2\mathrm{i}\sigma_z(\underline{x},t)\delta(\underline{x}-\underline{x}') \tag{A.5}$$

together with cyclic permutations of x, y and z.

The field operator $\mathbf{e}(\underline{x},t)$ is given by

$$\mathbf{e}(\underline{x},t) = \mathrm{i}\sum_{\underline{k},\lambda} \underline{g}_{\underline{k},\lambda}\left(a_{\underline{k},\lambda}(t)\mathrm{e}^{\mathrm{i}\underline{k}\cdot\underline{x}} - a^{\dagger}_{\underline{k},\lambda}(t)\mathrm{e}^{-\mathrm{i}\underline{k}\cdot\underline{x}}\right) \tag{A.6}$$

where $\underline{g}_{\underline{k},\lambda} = \sqrt{2\pi\hbar\omega_k/V_o}\;\hat{\epsilon}_{\underline{k},\lambda}$ and $\hat{\epsilon}_{\underline{k},\lambda}$ is a unit polarisation vector for mode $\underline{k}$ with polarisation index $\lambda = 1,2$. The quantisation volume V_o ($\to\infty$) contains the macroscopic region V and the atoms lie only in V. The field operators $a_{\underline{k},\lambda}$ and $a^{\dagger}_{\underline{k},\lambda}$ satisfy the relation

$$\left[a_{\underline{k},\lambda}(t), a^{\dagger}_{\underline{k}',\lambda'}(t)\right] = \delta_{\underline{k},\underline{k}'}\delta_{\lambda,\lambda'}. \tag{A.7}$$

The Heisenberg operator equations of motion according to the Hamiltonian (A.1) imply the following operator Bloch equations for the atomic operators,

$$\begin{aligned}\dot{\sigma_+}(\underline{x},t) &= \mathrm{i}\omega_o\sigma_+(\underline{x},t) + \mathrm{i}p\hbar^{-1}\hat{\underline{u}}\cdot\mathbf{e}(\underline{x},t)\sigma_z(\underline{x},t)\\ &= \left(\dot{\sigma_-}(\underline{x},t)\right)^{\dagger} \qquad \text{(A.8a)}\\ \dot{\sigma_z}(\underline{x},t) &= 2\mathrm{i}p\hbar^{-1}\hat{\underline{u}}\cdot\mathbf{e}(\underline{x},t)\left(\sigma_+(\underline{x},t)-\sigma_-(\underline{x},t)\right) \qquad \text{(A.8b)}\end{aligned}$$

where $\sigma_{\pm} = \frac{1}{2}(\sigma_x \pm \mathrm{i}\sigma_y)$ and we have used the fact that field and matter operators commute at the same time. Within the normally ordered prescription for placing the field operator $\mathbf{e}(\underline{x},t) \equiv \mathbf{e}^{+}(\underline{x},t) + \mathbf{e}^{-}(\underline{x},t)$ with respect to the atomic operators $\sigma_{\pm,z}(\underline{x},t)$ (*i.e.* the negative and positive frequency parts $\mathbf{e}^{\mp}(\underline{x},t)$ are placed to the left and right of the atomic operators, respectively) the operator Bloch equations (A.8) take the form,

$$\dot{\sigma_+}(\underline{x},t) - \mathrm{i}\omega_o\sigma_+(\underline{x},t) = \mathrm{i}p\hbar^{-1}\hat{\underline{u}}\cdot\mathbf{e}^{-}(\underline{x},t)\sigma_z(\underline{x},t) \tag{A.9}$$

$$\dot{\sigma_-}(\underline{x},t) + \mathrm{i}\omega_o\sigma_-(\underline{x},t) = -\mathrm{i}p\hbar^{-1}\hat{\underline{u}}\cdot\sigma_z(\underline{x},t)\mathbf{e}^{+}(\underline{x},t) \tag{A.10}$$

$$\begin{aligned}\dot{\sigma_z}(\underline{x},t) = -2\mathrm{i}p\hbar^{-1}\hat{\underline{u}}\cdot[&\mathbf{e}^{-}(\underline{x},t)\sigma_-(\underline{x},t)\\ &- \sigma_+(\underline{x},t)\mathbf{e}^{+}(\underline{x},t)].\end{aligned} \tag{A.11}$$

In equations (A.9, A.10) the terms in $\sigma_z(\underline{x},t)\mathbf{e}^{+}(\underline{x},t)$ and $\mathbf{e}^{-}(\underline{x},t)\sigma_z(\underline{x},t)$ are discarded within the rotating wave approximation (r.w.a.). Similarly, the terms in $\mathbf{e}^{-}(\underline{x},t)$ $\sigma_+(\underline{x},t)$ and $\sigma_-(\underline{x},t)\,\mathbf{e}^{+}(\underline{x},t)$ are dropped in (A.11).

From the Hamiltonian (A.1) it can be shown that the total field operator $\mathbf{e}(\underline{x},t)$, equation (A.6), satisfies Maxwell's wave equation as an operator form driven by $-4\pi c^{-2}\,\partial^2\underline{p}(\underline{x},t)/\partial t^2$ [25,26]. The equivalent integral form of the Maxwell's wave equation is given by [25,26]

$$\mathbf{e}(\underline{x},t) = \mathbf{e}_o(\underline{x},t) + \int_0^t \mathrm{d}t'\int_V \mathbf{F}(\underline{x},\underline{x}';t-t')\cdot\underline{p}(\underline{x}',t')\mathrm{d}\underline{x}' \tag{A.12}$$

in which $\mathbf{e}_o(\underline{x},t) = \mathbf{e}^{+}_o(\underline{x},t) + \mathbf{e}^{-}_o(\underline{x},t)$ is the free field operator where $\mathbf{e}^{\pm}_o(\underline{x},t)$ are given by

$$\mathbf{e}^{\pm}_o(\underline{x},t) = \pm\mathrm{i}\sum_{\underline{k},\lambda}\underline{g}_{\underline{k},\lambda}\left\{\begin{array}{c}a_{\underline{k},\lambda}(0)\\ a^{\dagger}_{\underline{k},\lambda}(0)\end{array}\right\}\mathrm{e}^{\mp\mathrm{i}(\omega_k t - \underline{k}\cdot\underline{x})}. \tag{A.13}$$

The second rank tensor photon propagator (or Green's function) $\mathbf{F}$ is given by the causal form ($t > t'$) (*cf.* [27])

$$\mathbf{F}(\underline{x},\underline{x}';t-t') = (\nabla_x\nabla_x - \nabla^2\mathbf{U})\delta(t-t'-rc^{-1})r^{-1} \tag{A.14}$$

where $r = |\underline{x}-\underline{x}'| \neq 0$ and $\mathbf{U}$ is the unit tensor. Its Fourier transform is given by ([25–29])

$$\mathbf{F}(\underline{x},\underline{x}';\omega) = (\nabla\nabla + (\omega/c)^2\mathbf{U})\mathrm{e}^{\mathrm{i}\omega rc^{-1}}r^{-1}. \tag{A.15}$$

In the extended system, the operator field $\mathbf{e}(\underline{x}_i,t) = \mathbf{e}^{+}(\underline{x}_i,t) + \mathbf{e}^{-}(\underline{x}_i,t)$ drives the atom i at site $\underline{x}_i$ where the positive and negative frequency parts $\mathbf{e}^{\pm}(\underline{x}_i,t)$ are expressed as the sum of three parts ([28]; see also [24,30]),

$$\mathbf{e}^{\pm}(\underline{x}_i,t) = \mathbf{e}^{\pm}_o(\underline{x}_i,t) + \mathbf{e}^{\pm}_{\mathrm{self}}(\underline{x}_i,t) + \mathbf{e}^{\pm}_{\mathrm{int}}(\underline{x}_i,t) \tag{A.16}$$

where the free field operators $\mathbf{e}^{\pm}_o$ are given by (A.13), while the self (reaction) field operators $\mathbf{e}^{\pm}_{\mathrm{self}}(\underline{x}_i,t)$ are given either within the integral term in (A.12) as $\int \underline{p}(\underline{x}).\mathbf{F}(\underline{x},\underline{x}';\omega)\delta(\underline{x}-\underline{x}')\mathrm{d}\underline{x}'$ [25,27,28] or within operator reaction field theory [31,32] (up to ignoring terms involving the vacuum level shifts) by

$$\mathbf{e}^{\pm}_{\mathrm{self}}(\underline{x}_i,t) = \pm\mathrm{i}\frac{2}{3}(\omega_o/c)^3\underline{p}\sigma^i_{\pm}(t). \tag{A.17}$$

The remaining operator terms $\mathbf{e}^{\pm}_{\mathrm{int}}(\underline{x}_i,t)$ in (A.16) are the internal field operators acting on atom i at $\underline{x}_i$ due to all the atoms $j \neq i$. The total internal field $\mathbf{e}_{\mathrm{int}}(\underline{x},t)$ carries the propagating field through the macroscopic system *i.e.* the cavity. In view of the inclusion of the self field in (A.16), the total internal propagating field $\mathbf{e}_{\mathrm{int}}(\underline{x},t)$ has the form of the integral term in (A.12) *but* with $\underline{x} \neq \underline{x}'$. It is this propagating field (not the free or self fields) that satisfies Maxwell's wave equation *driven* by $-4\pi c^{-2}\partial^2\underline{p}(\underline{x},t)/\partial t^2$ (although *cf.* [33], one should really *define* a macroscopique Maxwell field in the theory which *admits* $x = x'$). Up to the neglect of slow retardation effects and within slowly varying approximation in time $O(\omega_{\mathrm{c}}^{-1})$ for the atomic operators $\sigma_{\pm}(\underline{x},t)$ the total internal propagating fields at a single frequency, say, ω_{c}, $\mathbf{e}^{\pm}_{\mathrm{int}}(\underline{x},t)$, take the form [24,26]

$$\mathbf{e}^{\pm}_{\mathrm{int}}(\underline{x},t) = p\int_{\substack{V\\(\underline{x}\neq\underline{x}')}}\mathrm{d}\underline{x}'\sigma_{\mp}(\underline{x}',t)\hat{\underline{u}}\cdot\left\{\begin{array}{l}\mathbf{F}(\underline{x},\underline{x}';\omega_{\mathrm{c}})\\ \mathbf{F}^{*}(\underline{x},\underline{x}';\omega_{\mathrm{c}})\end{array}\right. . \tag{A.18}$$

Now, with the self fields given by (A.17) and the use of the algebraic relations for single atoms: $\sigma^i_+(t)\sigma^i_z(t) = -\sigma^i_+(t)$,

$\sigma_z^i(t)\sigma_-^i(t) = -\sigma_-^i(t)$ and $\sigma_+^i(t)\sigma_-^i(t) = (1/2)(1+\sigma_z^i(t))$ we get the following expressions [24]

$$\begin{aligned} \mathrm{i}p\hbar^{-1}\hat{\underline{u}}\cdot\mathbf{e}^-_{\mathrm{self}}(\underline{x},t)\sigma_z(\underline{x},t) &= -\frac{\gamma}{2}\sigma_+(\underline{x},t) \\ -\mathrm{i}p\hbar^{-1}\hat{\underline{u}}\cdot\sigma_z(\underline{x},t)\mathbf{e}^-_{\mathrm{self}}(\underline{x},t) &= -\frac{\gamma}{2}\sigma_-(\underline{x},t) \\ -2\mathrm{i}p\hbar^{-1}\hat{\underline{u}}\cdot[\mathbf{e}^-_{\mathrm{self}}(\underline{x},t)\sigma_-(\underline{x},t) - \sigma_+(\underline{x},t)\mathbf{e}^+_{\mathrm{self}}(\underline{x},t)] & \\ = -\gamma(I(\underline{x}) + \sigma_z(\underline{x},t)) & \end{aligned} \tag{A.19}$$

where $I(\underline{x}) = \sum_{i=1}^{N_a}\delta(\underline{x}-\underline{x}_i)$ and $\gamma = 4\,p^2\hbar^{-1}\omega_o^3/(3c^3)$ is the A-coefficient.

Using the expressions for $\mathbf{e}^{\pm}(\underline{x},t)$ as in (A.16) and equation (A.19) into the operator Bloch equations (A.9–A.11) we get

$$\dot{\sigma_+}(\underline{x},t) + (\frac{\gamma}{2} - \mathrm{i}\omega_o)\sigma_+(\underline{x},t) = \mathrm{i}p\hbar^{-1}\hat{\underline{u}}\cdot\mathbf{e}_o^-(\underline{x},t)\sigma_z(\underline{x},t) + \varepsilon^-_{\mathrm{int}}(\underline{x},t)\sigma_z(\underline{x},t) \tag{A.20a}$$

$$\dot{\sigma_-}(\underline{x},t) + (\frac{\gamma}{2} + \mathrm{i}\omega_o)\sigma_-(\underline{x},t) = -\mathrm{i}p\hbar^{-1}\hat{\underline{u}}\cdot\sigma_z(\underline{x},t)\mathbf{e}_o^+(\underline{x},t) + \sigma_z(\underline{x},t)\varepsilon^+_{\mathrm{int}}(\underline{x},t) \tag{A.20b}$$

$$\begin{aligned} \dot{\sigma_z}(\underline{x},t) + \gamma(I(\underline{x}) + \sigma_z(\underline{x},t)) = & \\ -2\mathrm{i}p\hbar^{-1}\hat{\underline{u}}\cdot\left[\mathbf{e}_o^-(\underline{x},t)\sigma_-(\underline{x},t) - \sigma_+(\underline{x},t)\mathbf{e}_o^+(\underline{x},t)\right] & \\ -2\left[\varepsilon^-_{\mathrm{int}}(\underline{x},t)\sigma_-(\underline{x},t) + \sigma_+(\underline{x},t)\varepsilon^+_{\mathrm{int}}(\underline{x},t)\right] & \end{aligned} \tag{A.20c}$$

where $\varepsilon^-_{\mathrm{int}}(\underline{x},t) = \mathrm{i}p\hbar^{-1}\hat{\underline{u}}\cdot\mathbf{e}^-_{\mathrm{int}}(\underline{x},t) = (\varepsilon^+_{\mathrm{int}}(\underline{x},t))^\dagger$, and for the terms on the r.h.s. in $\mathbf{e}_o^{\pm}(\underline{x},t)$ and $\varepsilon^{\pm}_{\mathrm{int}}(\underline{x},t)$ we have used the property that $\mathbf{e}(\underline{x}_i,t)\delta(\underline{x}-\underline{x}_i) = \mathbf{e}(\underline{x},t)\delta(\underline{x}-\underline{x}_i)$.

The free field annihilation and creation operators $a_{\underline{k},\lambda}(0)$ and $a^\dagger_{\underline{k},\lambda}(0)$ are operating on the state vector characterising the broad-band squeezed vacuum field. For one-dimensional space the correlation between mode pairs (labelled by ω,ω') of this squeezed vacuum are (*cf.* [12])

$$\langle a^\dagger(\omega)a(\omega')\rangle = N(\omega)\delta(\omega-\omega') \tag{A.21a}$$

$$\langle a(\omega)a(\omega')\rangle = M(\omega)\delta(\omega+\omega'-2\omega_{\mathrm{p}}) \tag{A.21b}$$

and

$$\langle a(\omega)\rangle = \langle a^\dagger(\omega)\rangle = 0. \tag{A.21c}$$

The parameter $N(\omega)$ represents the average photon number at frequency ω and $M(\omega)$ is a measure of the degree of squeezing (*i.e.* the amount of correlation between the sidebands at frequencies ω, $2\omega_{\mathrm{p}}-\omega$ where ω_{p} is the carrier (central) frequency of the squeezed vacuum [8–12]) with $|M(\omega)| \le \sqrt{N(\omega)(N(\omega)+1)}$, (generalisations to isotropic 3-dimensional correlated models were discussed in [34]; and references therein).

Having specified the correlation functions for the squeezed vacuum, we first outline the derivation for the mean atomic inversion $\bar{\sigma}_z(\underline{x},t) = \langle\sigma_z(\underline{x},t)\rangle$ where $|\ \rangle = |\mathrm{atom}\rangle\otimes|\mathrm{sq.vac.}\rangle$ is the combined state for the atoms and the (free) squeezed vacuum field. We integrate formally the operator equation for $\sigma_+(\underline{x},t)$, equation (A.20a) and substitute the result into the square bracket containing the free field operators terms $\mathbf{e}_o^{\pm}$ in equation (A.20c). Up to $O(e^2)$ (e is the electron charge, where p is proportional to the electronic charge) and within statistical decorrelation between field and matter terms which results in isolating the free field correlation functions equation (A.21) (*cf.* [34] for detail) we get

$$\dot{\bar{\sigma}_z}(\underline{x},t) + \gamma(I(\underline{x}) + \bar{\sigma}_z(\underline{x},t)) = -A - 2\langle\left[\varepsilon^-_{\mathrm{int}}(\underline{x},t)\sigma_-(\underline{x},t) + \sigma_+(\underline{x},t)\varepsilon^+_{\mathrm{int}}(\underline{x},t)\right]\rangle \tag{A.22}$$

where

$$A = 2p^2\hbar^{-2}\underline{u}\cdot\left[\int_0^t \mathrm{e}^{-\eta\tau}\bar{\sigma}_z(\underline{x},t')\times\langle\mathbf{e}_o^-(\underline{x},t')\mathbf{e}_o^+(\underline{x},t')\rangle\mathrm{d}t' + c.c.\right]; \tag{A.22a}$$

$\eta = \gamma/2 - \mathrm{i}\omega_o$, $\tau = t-t'$. With the free fields $\mathbf{e}_o^{\pm}(\underline{x},t')$, equation (A.13), and the use of the correlation functions (A.21a, A.21c) and after performing the integration over ω_k in the usual continuum limit and within the Markov approximation [34] we get finally

$$A = -2\gamma N\bar{\sigma}_z(\underline{x},t) \tag{A.23}$$

where $N = N(\omega=\omega_o)$. Thus (A.22) becomes

$$\begin{aligned} \dot{\bar{\sigma}_z}(\underline{x},t) = & -\gamma(I(\underline{x}) + (1+2N)\bar{\sigma}_z(\underline{x},t)) \\ & -2\left[\langle\varepsilon^-_{\mathrm{int}}(\underline{x},t)\rangle\bar{\sigma}_-(\underline{x},t) + c.c.\right] \end{aligned} \tag{A.24}$$

where in (A.24) we have (semiclassically) decorrelated the terms $\langle\varepsilon^-_{\mathrm{int}}(\underline{x},t)\sigma_-(\underline{x},t)\rangle \approx \langle\varepsilon^-_{\mathrm{int}}(\underline{x},t)\rangle\bar{\sigma}_-(\underline{x},t)$ and $\langle\sigma_+(\underline{x},t)\varepsilon^+_{\mathrm{int}}(\underline{x},t)\rangle \approx \langle\varepsilon^+_{\mathrm{int}}(\underline{x},t)\rangle\bar{\sigma}_+(\underline{x},t)$.

Following the same procedure, by formally integrating equation (A.20c) for $\sigma_z(\underline{x},t)$ and inserting the result into equation (A.20a) for $\sigma_+(\underline{x},t)$ and the use of the squeezed vacuum correlations (A.21b) and up to $O(e^2)$ and within the same approximations as before we get finally [30,34]

$$\begin{aligned} \dot{\bar{\sigma}_+}(\underline{x},t) = & -(\frac{\gamma}{2}(1+2N) - \mathrm{i}\omega_o)\bar{\sigma}_+(\underline{x},t) \\ & -\gamma M(\underline{x})\mathrm{e}^{2\mathrm{i}\omega_{\mathrm{p}}t}\bar{\sigma}_-(\underline{x},t) - \langle\varepsilon^-_{\mathrm{int}}(\underline{x},t)\rangle\bar{\sigma}_z(\underline{x},t) \end{aligned} \tag{A.25}$$

where $M(\underline{x}) = M\mathrm{e}^{-2\mathrm{i}k_{\mathrm{p}}x}$ ($k_{\mathrm{p}} = \omega_{\mathrm{p}}c^{-1}$) for a correlated squeezed vacuum along the x-direction orthogonal to the cavity z-axis [35]. Note $M(\underline{x}) = \textit{constant}$, say M, with respect to any variation along the z-direction (the case of our concern). Thus with this in mind, and in a rotating frame at the input field frequency ω_{d} and for $\omega_{\mathrm{p}} = \omega_{\mathrm{d}}$ the

c-number Bloch equations (A.24, A.25) are of the form

$$\begin{aligned}\dot{\bar{\sigma}}_+(\underline{x},t) &= -(\frac{\gamma}{2}(1+2N)+\mathrm{i}\delta)\bar{\sigma}_+(\underline{x},t) - \gamma M\bar{\sigma}_-(\underline{x},t) \\ &\quad - \langle\bar{\varepsilon}^-_{\mathrm{int}}(\underline{x},t)\rangle\bar{\sigma}_z(\underline{x},t) \\ &= \left(\dot{\bar{\sigma}}_-(\underline{x},t)\right)^* \qquad \text{(A.26a)} \\ \dot{\bar{\sigma}}_z(\underline{x},t) &= -\gamma(I(\underline{x})+(1+2N)\bar{\sigma}_z(\underline{x},t)) \\ &\quad - 2\left[\langle\bar{\varepsilon}^-_{\mathrm{int}}(\underline{x},t)\rangle\bar{\sigma}_-(\underline{x},t)+c.c\right]. \qquad \text{(A.26b)}\end{aligned}$$

Finally the c-number equations (A.26) are to be ensemble averaged over the sites $\underline{x}_i$ [24,30] by setting

$$\begin{aligned}J_\pm(\underline{x},t) &= n_o^{-1}\langle\bar{\sigma}_\pm(\underline{x},t)\rangle_{\mathrm{Avr.}} \\ 2J_z(\underline{x},t) &= n_o^{-1}\langle\bar{\sigma}_z(\underline{x},t)\rangle_{\mathrm{Avr.}} \qquad \text{(A.27)}\end{aligned}$$

where $n_o \equiv \langle\sum_{i=1}^{N_a}\delta(\underline{x}-\underline{x}_i)\rangle_{\mathrm{Avr.}} \equiv \langle I(\underline{x})\rangle_{\mathrm{Avr.}}$ is the mean number density of atoms obtained after an ensemble average over the sites $\underline{x}_i \in V$ and $\langle\bar{\sigma}_{\pm,z}(\underline{x},t)\rangle_{\mathrm{Avr.}}$ are ensemble averages of the quantum mean values of the full operators $\sigma_{\pm,z}(\underline{x},t)$ scaled to a single atom. For the ensemble average, concerning products like

$$\begin{aligned}&\left\langle\langle\bar{\varepsilon}^-_{\mathrm{int}}(\underline{x},t)\rangle\bar{\sigma}_z(\underline{x},t)\right\rangle_{\mathrm{Avr.}} = \\ &\mathrm{i}p^2\hbar^{-1}\int\limits_{\substack{V\\(\underline{x}\neq\underline{x}')}}\mathrm{d}\underline{x}'\underline{\hat{u}\hat{u}}:\mathbf{F}(\underline{x},\underline{x}';\omega_{\mathrm{c}})\left\langle\bar{\sigma}_+(\underline{x}',t)\bar{\sigma}_z(\underline{x},t)\right\rangle_{\mathrm{Avr.}}\end{aligned}$$

we set

$$\langle\bar{\sigma}_+(\underline{x}',t)\bar{\sigma}_z(\underline{x},t)\rangle_{\mathrm{Avr.}} = g(r)J_+(\underline{x}',t)(2J_z(\underline{x},t)) \qquad \text{(A.28)}$$

where $g(r)$ is the two-body correlation function [28]

$$g(r) = n_o^{-2}\left\langle\sum_{\substack{i,j=1\\i\neq j}}^{N_a}\delta(\underline{x}-\underline{x}_i)\delta(\underline{x}'-\underline{x}_j)\right\rangle_{\mathrm{Avr.}} \qquad \text{(A.29)}$$

and $r = |\underline{x}-\underline{x}'|$.

Correlation functions of all orders appear in the linear dielectric theory [28,33], and for low atomic density we can take $g(r)\approx 1$ [25,33].

Thus with the ensemble average as described and for low atomic density, the ensemble averaged Bloch equations (A.26) are exactly the equations (2b, 2c), with $\langle\bar{\varepsilon}^+_{\mathrm{int}}(\underline{x},t)\rangle$ identified (after ensemble average) as α, *i.e.*

$$\alpha = -\mathrm{i}n_o p^2\hbar^{-1}\int\limits_{\substack{V\\(\underline{x}\neq\underline{x}')}}\mathrm{d}\underline{x}'\underline{\hat{u}\hat{u}}:\mathbf{F}^*(\underline{x},\underline{x}';\omega_{\mathrm{c}})J_-(\underline{x}',t). \qquad \text{(A.30)}$$

As noted this internal propagating cavity field satisfies the full Maxwell's wave equation *driven* by $-4\pi c^{-2}\,\partial^2 J_-(\underline{x},t)/\partial t^2$. Within the slowly varying approximation in space and time (*e.g.* [9]) the full Maxwell's wave equation is replaced by the reduced equation (2a) for the field $\alpha(z,t)$.

Appendix B

In this appendix we show that in the dispersive case where both $|\theta|$, $|\delta| \gg 1$ and for $C \gg 1$ and small N the boundary of the bistable region is approximated by one of the two hyperbolas of equation (20).

If $|\theta| \gg 1$, $|\delta| \gg 1$ and N is small then $|D_1| \gg 1$, $|D_1\theta| \gg 1$ and the condition (10b) which requires that $f(\theta,\delta) > 0$, gives from equation (11) that,

$$\left(\left(\frac{CD_1^2}{D_2}\right)+\theta D_1\right)^3 - \frac{27}{4}\left(\frac{CD_1^2}{D_2}\right)(\theta D_1)^2 \geq 0 \qquad \text{(B.1)}$$

which simplifies to

$$\left(2\frac{CD_1^2}{D_2}-\theta D_1\right)^2\left(\frac{CD_1^2}{4D_2}+\theta D_1\right)\geq 0. \qquad \text{(B.2)}$$

So, from (B.2) we have,

$$\frac{\theta D_2}{D_1} \leq 2C \quad \text{if} \quad D_1\theta > 0 \qquad \text{(B.3a)}$$

and

$$\frac{\theta D_2}{D_1} \geq -\frac{C}{4} \quad \text{if} \quad D_1\theta < 0. \qquad \text{(B.3b)}$$

For $|\delta| \gg 1$, we have

$$\begin{aligned}\frac{D_2}{D_1} &= \frac{(1+\delta^2)(1+2N)}{\delta\left[1+\dfrac{2|M|}{\delta}\sin\phi\right]} \\ &\approx (1+2N)(\delta-2|M|\sin\phi) \qquad \text{(B.4)}\end{aligned}$$

which is a good approximation as $|M| \leq \sqrt{N(N+1)}$ and N small. Thus the conditions (B.3) reduce to

$$\theta(\delta-\delta_o) \leq \frac{2C}{1+2N}; \quad D_1\theta > 0 \qquad \text{(B.5a)}$$

$$\theta(\delta-\delta_o) \geq \frac{-C}{4(1+2N)}; \quad D_1\theta < 0, \qquad \text{(B.5b)}$$

where $\delta_o = 2|M|\sin\phi$. For consistency equation (B.3) require that $C \gg 1$. In the normal vacuum case ($N = M = 0$) these reduce to

$$\theta\delta \leq 2C \quad \text{if} \quad \delta\theta > 0 \qquad \text{(B.6a)}$$

$$\theta\delta \geq \frac{-C}{4} \quad \text{if} \quad \delta\theta < 0 \qquad \text{(B.6b)}$$

as given in [18].

Conditions (B.5) define a region of bistability whose boundary is approximated by the two hyperbolas,

$$\begin{aligned}\theta(\delta-\delta_o) &= \frac{2C}{1+2N} \quad \text{if} \quad D_1\theta > 0, \\ \theta(\delta-\delta_o) &= \frac{-C}{4(1+2N)} \quad \text{if} \quad D_1\theta < 0. \qquad \text{(B.7)}\end{aligned}$$

In the regions of the plane where (B.5a) holds, and from equation (9), we have $X_{\rm inf} \geq 0$. Equality holds on the hyperbolic boundary of this region so bistability is possible within the region enclosed by the hyperbola. Similarly $X_{\rm inf} > 0$ in the region of the plane where (B.5b) holds.

Note that, these hyperbolas are approximate boundary of the bistability region if $|\theta| \gg 1$, $|\delta| \gg 1$. *In practice*, the boundary will cut the θ- and δ-axes. Now, we determine these points of intersection for $C \gg 1$ and small N.

For $\theta = 0$ the condition (10b) (*i.e.* $f(\theta, \delta) > 0$) gives

$$(CD_1^2 - D_2)^3 - \frac{27}{4} CD_2^2 D_1^4 \geq 0. \tag{B.8}$$

For $C \gg 1$, and small N, $CD_1^2 \gg D_2$ hence (B.8) reduces to

$$\left(\frac{D_2}{D_1}\right)^2 \leq \frac{4}{27} C^2. \tag{B.8a}$$

By using the approximation of equation (B.4) for $\delta \gg 1$ we have then the extrema of δ given by equation (21), *i.e.*

$$(\delta^{\pm})_{\theta=0} = 2|M| \sin\phi \pm C\sqrt{\frac{4}{27}}(1+2N)^{-1}. \tag{B.9}$$

Similarly the condition (10b) for $D_1 = 0$ (*i.e.* $\delta = -\delta_o$) and $C \gg 1$ gives

$$|\theta| \leq \sqrt{\frac{4}{27}} \frac{C}{D_2} \tag{B.10}$$

where D_2 is evaluated at $\delta = -\delta_o$, and the extrema of θ are then given by equation (22), *i.e.*

$$(\theta^{\pm})_{\delta=-\delta_o} = \pm C\sqrt{\frac{4}{27}} \frac{\left[1 - \dfrac{2|M|}{1+2N}\cos\phi\right]}{1+\delta_o^2}. \tag{B.11}$$

References

1. R.L. Sutherland, *Handbook of Nonlinear Optics* (Marcel Dekker Inc., N.Y., 1996).
2. *Optical Computing*, edited by B.S. Wherrett, P. Chavel (Inst. of Physics Publ., Bristol, 1995).
3. *Design Issues in Optical Processing*, edited by J.N. Lee (Cambridge Univ. Press, Cambridge, U.K., 1995).
4. D.G. Feitelson, *Optical Computing* (MIT Press, Mass., 1988).
5. P. Mandel, *Theoretical problems in Cavity Nonlinear Optics* (Cambridge Univ. Press, Cambridge, U.K., 1997).
6. L.A. Lugiato, L.M. Narducci, in *Fundamental Systems in Quantum Optics*, edited by J. Dalibard, J.M. Raimond, J. Zinn-Justin (Elsevier Sci. Publ., Amsterdam, 1992), pp. 942-1043.
7. H.J. Kimble, G.L. Oppo, in *Quantum Dynamics of Simple Systems* (Inst. of Physics Publ., London, 1996), pp. 183-198.
8. H.J. Kimble, in reference [6] pp. 545-674 (also see other relevant articles in [6]).
9. L. Mandel, E. Wolf, *Optical Coherence and Quantum Optics* (Cambridge Univ. Press, Cambridge, U.K., 1995).
10. M.O. Scully, M.S. Zubairy, *Quantum Optics* (Cambridge Univ. Press, Cambridge, U.K., 1997).
11. D.F. Walls, G.J. Milburn, *Quantum Optics* (Springer, Berlin, 1995).
12. C.W. Gardiner, Phys. Rev. Lett. **56**, 1917 (1986).
13. S.F. Hass, M. Sargent III, Opt. Commun. **79**, 366 (1990).
14. P. Galatola, L.A. Lugiato, M. Porreca, P. Tombesi, Opt. Commun. **81**, 175 (1991).
15. J. Bergou, D. Zhao, Phys. Rev. A **52**, 1550 (1995).
16. R. Bonifacio, L.A. Lugiato, Lett. Nuovo Cimento **21**, 505 (1978).
17. R. Bonifacio, L.A. Lugiato, Opt. Commun. **19**, 172 (1976).
18. S.S. Hassan, P.D. Drummond, D.F. Walls, Opt. Commun. **27**, 480 (1978).
19. R. Bonifacio, M. Gronchi, L.A. Lugiato, Nuovo Cimento **53**, 311 (1979); R. Bonifacio, L.A. Lugiato, Lett. Nuovo Cimento **21**, 517 (1978).
20. S.M. Maize, M.F. Ali, S.S. Hassan, Nonlinear Opt. **8**, 219 (1994).
21. J.A. Fleck, Appl. Phys. Lett. **13**, 365 (1968).
22. S.L. McCall, Phys. Rev. A **9**, 1515 (1974); S.L. McCall, H.M. Gibbs, Opt. Commun. **33**, 335 (1980).
23. J.D. Murray, *Mathematical Biology* (Springer-Verlag, Berlin, 1993), Chap. 5.
24. S.S. Hassan, R.K. Bullough, in *Optical Bistability*, edited by C.M. Bowden, M. Ciftan, H.R. Robl (Plenum Press, N.Y., 1981), pp. 367-404.
25. R.K. Bullough, J. Phys. A. **1**, 409 (1968); **2**, 477; **3**, 708, 726, 751 (1970); F. Hynne, R.K. Bullough, J. Phys. A. **5**, 1272 (1972).
26. R. Saunders, Ph.D. thesis, University of Manchester, 1973; S.S. Hassan, Ph.D. thesis, University of Manchester, 1976.
27. J.D. Jackson, *Classical Electrodynamics*, 2nd edn. (John Wiley, N.Y., 1975).
28. L. Rosenfield, *Theory of Electrons* (Dover Publ. Inc., N.Y., 1965).
29. R.K. Bullough, S.S. Hassan, Proc. SPIE **369**, 257 (1982).
30. S.S. Hassan, R.K. Bullough, H.A. Batarfi, in *Studies in Classical and Quantum nonlinear optics*, edited by O. Keller (Nova Sci. Publ. Inc., N.Y., 1995), pp. 609-623.
31. R. Saunders, R.K. Bullough, F. Ahmad, J. Phys. A **8**, 759 (1975).
32. J.R. Ackerhalt, J.H. Eberly, Phys. Rev. D **10**, 3350 (1974).
33. F. Hynne, R.K. Bullough, Phil. Trans. Roy. Soc. Lond. A **312**, 251 (1984); *ibid.* **321**, 305 (1987); *ibid.* **330**, 253 (1990).
34. S.S. Hassan, M.R. Wahiddin, R. Saunders, R.K. Bullough, Physica A **215**, 556; *ibid.* **219**, 482 (1995).
35. Implicitly, we reach a three-dimensional squeezed vacuum, and a three-dimensional, not a two-dimensional, theory by choosing a beam of squeezed light directed along the x-axis incident on the beam from the ring cavity travelling along the z-axis thus the one-dimensional squeezed vacuum, equations (A.21a–A.21c), has all its modes directed along the x-axis and is isotropic in all directions orthogonal to that direction. In [34] for example we consider arbitrary three-dimensional squeezed vacua of any geometry.